

## Super-Resolution Approach to Enhance Bone Marrow Trepine Image in the Classification of Classical Myeloproliferative Neoplasms

Umi Kalsom Mohamad Yusof<sup>1</sup>, Syamsiah Mashohor<sup>1\*</sup>, Marsyita Hanafi<sup>1</sup>, Sabariah Md Noor<sup>2</sup> and Norsafina Zainal<sup>3</sup>

<sup>1</sup>Department of Computer and Communication Systems Engineering, Faculty of Engineering Universiti Putra Malaysia, 43400 UPM, Serdang, Selangor, Malaysia

<sup>2</sup>Department of Pathology, Faculty of Medicine and Health Sciences, Universiti Putra Malaysia, 43400 UPM, Serdang, Selangor, Malaysia

<sup>3</sup>Pathology Department, Hospital Serdang, Jalan Puchong, 43000 Kajang, Selangor, Malaysia

### ABSTRACT

Many diseases require histopathology images to characterise biological components or study cell and tissue architectures. The histopathology images are also essential in supporting disease classification, including myeloproliferative neoplasms (MPN). Despite significant developments to improve the diagnostic tools, morphological assessment from histopathology images obtained by bone marrow trephine (BMT) remains crucial to confirm MPN subtypes. However, the assessment outcome is challenging due to subjective characteristics that are hard to replicate due to its inter-observer variability. Apart from that, image processing may reduce the quality of the BMT images and affect the diagnosis result. This study has developed a classification system for classical MPN subtypes: polycythemia vera (PV), essential thrombocythemia (ET), and primary myelofibrosis (MF). It was done by reconstructing low-resolution images of BMT using a super-resolution approach to address the issue. Identified low-resolution images from calculating Laplacian variance

were reconstructed using a super-resolution convolution neural network (SRCNN) to transform into rich information of high-resolution images. Original BMT images and reconstructed BMT images using the SRCNN dataset were fed into a CNN classifier, and the classifier's output for both datasets was compared accordingly. Based on the result, the dataset consisting of the reconstructed images showed better output

### ARTICLE INFO

#### Article history:

Received: 28 April 2022

Accepted: 07 September 2022

Published: 13 July 2023

DOI: <https://doi.org/10.47836/pjst.31.5.02>

#### E-mail addresses:

ukalsomyusof@gmail.com (Umi Kalsom Mohamad Yusof)

syamsiah@upm.edu.my (Syamsiah Mashohor)

marsyita@upm.edu.my (Marsyita Hanafi)

md\_sabariah@upm.edu.my (Sabariah Md Noor)

finazz8081@yahoo.com.my (Norsafina Zainal)

\* Corresponding author

with 92% accuracy, while the control images gave 88% accuracy. In conclusion, the high quality of histopathology images substantially impacts disease process classification, and the reconstruction of low-resolution images has improved the classification output.

*Keywords:* Artificial intelligence, histopathology images, image reconstruction, myeloproliferative neoplasm, super-resolution

## INTRODUCTION

Hematopoietic cells are developing blood cells in the bone marrow and are divided into three categories, each producing a different type of blood cell. Cells from all three lineages, namely erythroid, granulocytic, and megakaryocytic, are found in normal bone marrow, as shown in Figure 1, which refers to the normal production of certain white blood cells (WBC), red blood cells (RBC), and platelets.

Myeloproliferative neoplasms (MPN) are a group of diseases that perform clonal proliferation of bone marrow stem cells, which causes the increased production of platelets, WBC, or RBC in the circulation and sometimes causes marrow fibrosis with consequent of extramedullary haematopoiesis (cell production outside the marrow).

The concept of MPN was founded by William Dameshek in 1951 (Dameshek, 1951). However, critical advances in its proper understanding and approach have been happening in the recent 20 years (Arber et al., 2016; Tavares et al., 2019; Vannucchi & Harrison, 2017) with significant scientific advances have been attained with higher accuracy in diagnosis, new risk classifications, and therapeutic approach updates. Essential improvements were described in a document ‘WHO Classification of Hematopoietic and Lymphoid Tissue Tumors’ by the World Health Organization (WHO), including bone marrow histology, which advocates from a minor to a major diagnostic criterion (Barbui et al., 2018). Following the guidelines, the MPN entities were grouped into seven subtypes (Hasserjian, 2018), as shown in Table 1.

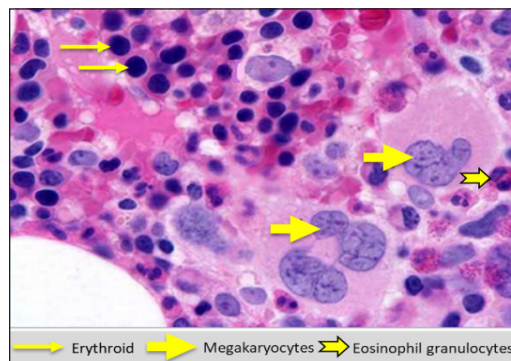


Figure 1. Elements of all three major cell lines are seen in an image of normal bone marrow

Table 1  
MPN subtypes

No	Diseases
1.	Chronic myeloid leukaemia (CML), BCR-ABL1-positive
2.	Chronic neutrophilic leukaemia (CNL)
3.	Polycythemia vera (PV)
4.	Primary myelofibrosis (MF)
5.	Essential thrombocythemia (ET)
6.	Chronic eosinophilic leukaemia (CEL), not otherwise specified (NOS)
7.	Myeloproliferative neoplasm, unclassifiable (MPN-U)

A genetic abnormality in the chromosome contains a fusion gene called BCR-ABL1, identified by a translocation (9;22) known as the Philadelphia chromosome (Ph). For example, a diagnosis with BCR-ABL1 positive indicates a CML type. On the other hand, BCR-ABL1-negative MPNs (also referred to as the classical MPNs) are PV, ET, and MF (Sirinukunwattana et al., 2019), and these three subtypes of MPN are encountered as the main scope in this study.

### **Quality of Data and Image Reconstruction**

Image quality is often neglected in the design of machine vision systems (Dodge & Karam, 2016). Usually, machine vision systems are trained and tested on high-quality image datasets, yet in practice, the input images are exposed to numerous factors that cause quality distortions. Blur images, for example, are among the undesirable effects that lead to the loss of necessary details. Automatic detection of blurred and sharp pixels in an image and their classification into respective regions are vital for different image processing and computer vision applications (Ali & Mahmood, 2018), including in medical applications. Medical image reconstruction has become one of the most fundamental and necessary medical imaging components in recent years, with the primary goal of obtaining high-quality medical images for clinical use at the lowest cost and risk to patients (Zhang & Dong, 2020). Leena and Sreenath's (2019) study applied blur detection in pre-processing stage by determining the score of blurriness using the Laplacian operator. The image is classified as blurred or non-blurred when the calculated score is less than the measured threshold. The major advantage of the technique is that it is less time-consuming because the output is yielded immediately within five to seven microseconds (Leena & Sreenath, 2019). Another approach is shown by Huang et al. (2018) using discriminative blur features via deep convolutional neural networks (DCNN). Six layers of the CNN model were developed with five layers for feature extraction for binary classification, which can faithfully produce patch-level blur likelihood. Multiscale image patches are extracted for each pixel by sliding window manner to detect an image. The final blur detection result is obtained by fusing multiscale blur probability maps (Huang et al., 2018). Despite the high performance at blur detection for single and multiple scales, this method consumes many training data and causes a real-time problem.

Generating a high-resolution image with the most commonly used and straightforward approach is by applying linear interpolation methods such as the nearest neighbour, bilinear, and bicubic interpolations (Parsania & Virparia, 2016). However, these approaches frequently result in over-smoothed images with artefacts like aliasing, blur, and halo around the edges (Umehara et al., 2018). Inspired by the success of deep learning in computer vision problems and medical image analysis, researchers have recently investigated deep learning approaches, including Super-resolution Convolutional Neural Network (SRCNN) and

Very Deep Convolutional Network (VDSR) for various biomedical image reconstruction problems (Chen et al., 2019; Cheng et al., 2018; Hou et al., 2020; Zhang et al., 2020). VDSR was developed based on the popular VGG network for image classification, where the VDSR consists of many convolutional layers with ReLU activation.

Hwang et al.'s (2018) study involved the application of VDSR to restore compressed images of cone beam computed tomography (CBCT) in the dental field. The output of the image shows more delicate details and a sharper edge. However, deeper networks in VDSR can bring drawbacks to overfitting and produce a vast model that needs high computational processing power (Hayat, 2017). Another SRCNN approach was applied in image enhancement, for instance, in computed tomography (CT) images. The outcome of an Umahera et al. (2018) experiment to enhance image resolution in the chest CT images demonstrated that the SRCNN significantly outperformed conventional linear interpolation methods. In the pandemic of COVID-19, predicting patients that have coronavirus was done via X-rays and CT-scans (Alzubaidi et al., 2021; Jain & Kosamkar, 2022). However, these images sometimes suffer blurriness or low visibility. Jain & Kosamkar (2022) transformed these low-visibility images into high-visibility images by applying super-resolution using SRCNN. As a result, the classification of COVID-19 attained an accuracy of 95.31%, which is higher than those without image super-resolution (ISR) (Jain & Kosamkar, 2022). Another study was shown by Taş and Yılmaz (2021) on automatic colonoscopy-based diagnosis and polyp detection and localisation. SRCNN pre-processing approach was used to increase the resolution of the training colonoscopy images. This method provides better results and reached an F2 score of 0.945 for the correct localisation of colon polyps compared to the low-resolution cases (Taş & Yılmaz, 2021).

## **METHODOLOGY**

This study consisted of a few stages, as shown in Figure 2. Data collection was prepared from online resources labelled 'validated by hematologist' followed by a data cleaning process. Then, data augmentation was implemented to increase the variety of images and expand the number of images in the dataset. Later, data quality was performed to check the blurry level, and the blurred images were reconstructed using SRCNN. The learning-based classification was performed to evaluate the efficiency of the SRCNN reconstruction method. Finally, the classification output between the control and reconstructed images was compared to observe the model performance.

### **Data Preparation**

In the advancement of the digitisation era nowadays (Mariam et al., 2022; Vasudevan et al., 2022), researchers can share datasets that are foreseen to benefit the academic community virtually. Every discovery and new finding can be shared globally, and anyone interested in

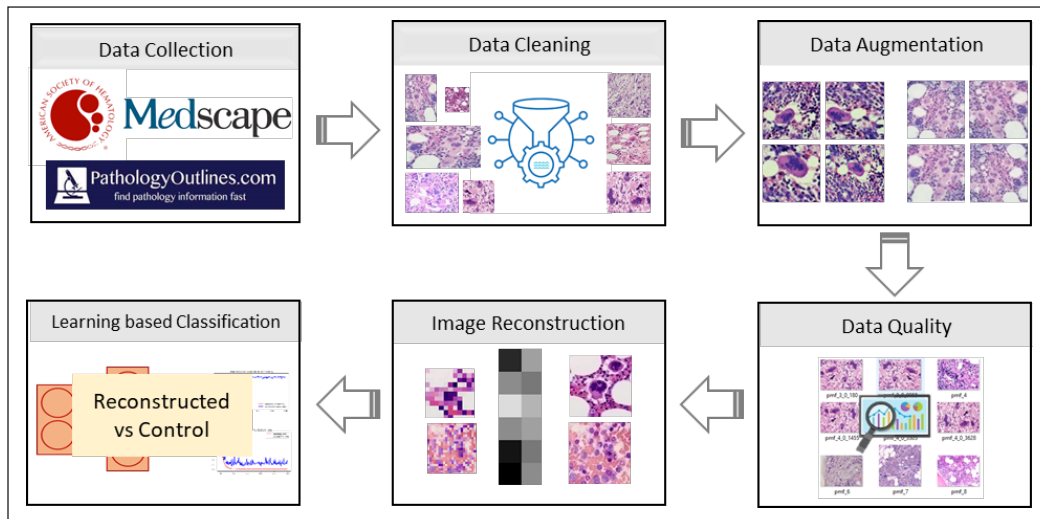


Figure 2. The flow of the study

the subject domain can access the information and contribute back through digital platforms. Similar circumstances were observed in the medical field, including haematology. Three platforms that provide shared information and free downloadable image dataset with expert peer review were chosen as data sources for data collection: The American Society of Haematology Image Bank (AHS), PathologyOutlines.com (Path.com), and Medscape. In total, 268 BMT images were collected, with 161 images from AHS, 67 from Path.com, and 40 from Medscape. The dataset was reviewed thoroughly, and similar images were filtered. A high possibility of duplicate images can occur for a similar disease type due to the open-sharing dataset's data sources. The image description from the data sources was also rechecked to confirm the inclusion and exclusion criteria. The selected BMT images were also observed to discriminate features based on the standardised morphological criteria in bone marrow specimens provided by WHO, such as bone marrow cellularity, formation of fibrosis, and megakaryopoiesis, including the size of cells, cluster formation, and nuclear features. These data cleaning and data checking processes were conducted with the guidance of a 10-year experienced haematologist.

### Bone Marrow Image Augmentation and Image Quality Checking

Some research has demonstrated the efficiency of deep learning in classifying images (Loey et al., 2020; Rahaman et al., 2021; Talo, 2019). However, these networks rely heavily on big-quality data to predict well. On the other hand, data augmentation is a critical strategy for enhancing generalisation ability when deep learning models are furnished with the original images and numerous image variants. This approach also has proven to prevent the memorisation of deep learning models efficiently and hence becomes a helpful

technique in improving the model's performance to predict real data. Therefore, data augmentation was applied to the dataset to expand the training dataset's size and enhance the images' variability. Transformations include a range of operations from the field of image manipulation, such as shifting (0.1 to 0.2), zooming (0.3 to 0.5), rotating (10 to 30 degrees), and flipping (horizontal and vertical), as presented in Figure 3.

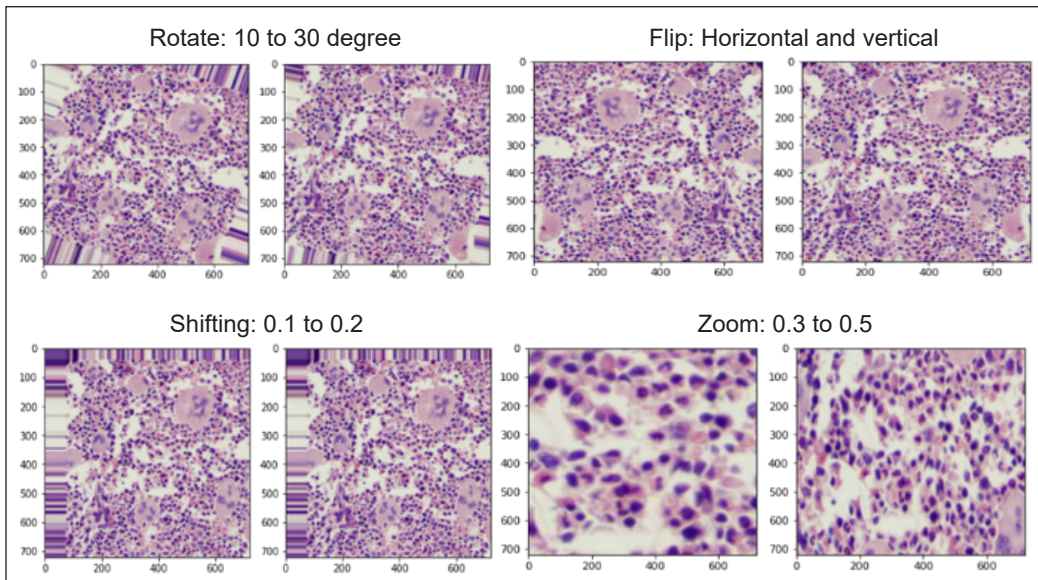


Figure 3. Augmentation output of samples of BMT image using rotating, flipping, shifting, and zooming manipulations

The augmentation applied to the images has successfully increased the dataset size, but it needed to be re-reviewed to observe the effect of the augmentation. The occurrence of low-quality images, such as blurry images with poor surrounding features and black padding with duplicated pixel values, was expected even after applying the preferred setting values. The expectation is that the augmentation happened randomly within the range setting, and the variety of positions of the features in the images may cause defects in the augmentation. From the observation, the undesirable images were removed. Moreover, with a suitable image frame, the images were cropped to the region of interest (ROI). Removing generated images with poor surrounding features and black padding with duplicated pixel values was unavoidable because it could cause the training process to feed unclean input and give wrong output predictions. Meanwhile, the blurry images underwent reconstruction to be transformed into high-quality images. The input was also carefully cropped to square as the deep learning model only receives square images as input.

Following the augmentation process, the quality checking of the bone marrow images in the dataset was done to identify low-resolution images. The working process for blur identification is presented in Figure 4.

The image source in RGB containing three channels of images was converted to grayscale images as a single-channel image. The purpose of the conversion was to simplify the calculation of Laplacian variance to calculate only a single channel of the image. Immediately after the conversion, the value of the Laplacian variance was computed using the Laplacian operator. The Laplacian operator is the second-order differential operator in  $n$ -dimensional Euclidean space. It is expressed as the divergence ( $\nabla$ ) of the gradient ( $\nabla f$ ). The Laplacian of  $f$  is the sum of the second partial derivatives in the Cartesian coordinates,  $x_i$ . The Laplacian variance was calculated for each image by applying Equation 1 to emphasise regions with rapid intensity changes. Lesser edges with a lower value of Laplacian variance were assumed to be blurred images. In contrast, high variance disclosed that there were more edge-like to imply a sharper type of image.

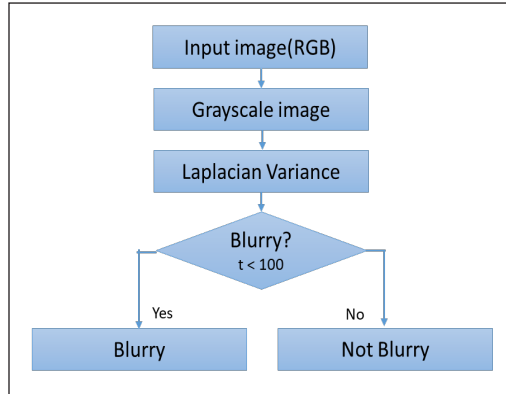


Figure 4. Blur detection flow in images dataset

$$\nabla^2 f = \sum_{i=1}^n \frac{\delta^2 f}{\delta x_i^2} \quad [1]$$

The default threshold value,  $t = 100$ , was set as a discriminant value to classify the image quality category. From the output, an image with a variance of less than 100 was categorised as ‘Blurry’; meanwhile, output for more or equal to 100 was identified as ‘Not Blurry’. The threshold value selection was referred to based on a previous study (Leena & Sreenath, 2019) and was observed in the data collection for suitability for implementation.

### Application of SRCNN to Blur Images

In implementing the image reconstruction, hardware and software parts were vigilantly prepared since the architecture is well known for high computational power. The program was run in a Colab notebook provided by Google Colaboratory (Colab). The model was scripted in Python (version Python 3) using the backend framework of TensorFlow and Keras. Colab is a jupyter notebook environment that provides a runtime that fully configures for deep learning and has free-of-charge access to a robust virtual GPU. A 12GB RAM is available, with the types of GPU vary over time. Often available GPU includes NVIDIA K80, T4, P4, and P100.

The SRCNN is a pioneering work in applying CNN to ISR reconstruction. It mainly implements end-to-end LR and HR image mapping, as shown in Figure 5 (Umehara et al., 2018).

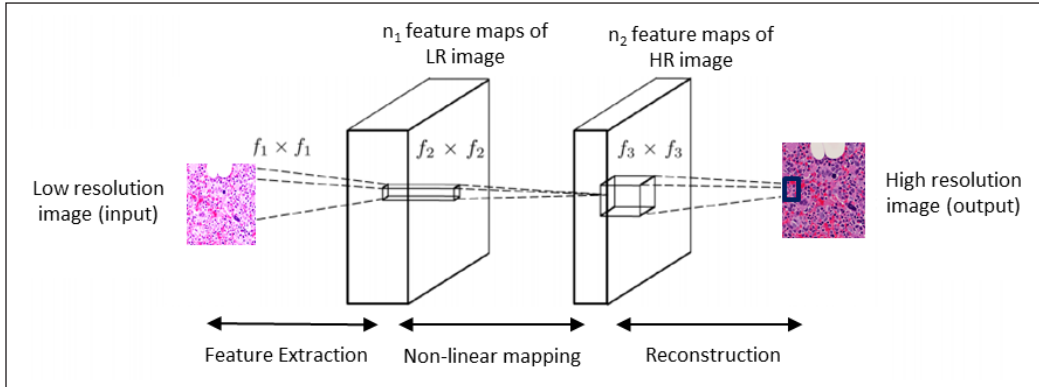


Figure 5. The architecture of SRCNN in BMT image reconstruction

The implementation of SRCNN consists of three processes. The low-resolution BMT images were fed as input to begin the image reconstruction as the first convolution with feature extraction to extract the image blocks, while the dimensions of feature vectors were still in low-dimensional space and expressed in Equation 2:

$$F_1(Y) = \max(0, W_1 * Y + B_1) \quad [2]$$

where  $F$  = mapping function,  $Y$  = bicubic interpolated low-resolution image,  $W_i$  = filters, and  $B_i$  = biases.

Followed by non-linear mapping in the second convolution, low-dimensional features were mapped to high-dimensional features. The second layer maps  $n_1$  – dimensional, the representations (feature vectors) of several patches, into  $n_2$  – dimensional, resulting in a non-linear mapping. The number of patches for each mapping operation depends on the kernel size of the second convolution layer, and the operation for this stage is stated as in Equation 3:

$$F_2(Y) = \max(0, W_2 * F_1(Y) + B_2) \quad [3]$$

where  $W_2$  with the size of  $n_1 \times f_2 \times f_2$  corresponds to  $n_2$  filters and  $B_2$  as  $n_2$ -dimensional vector.

Subsequently, the image reconstruction where the process was equivalent to the convolution used the mean convolution kernel with the final operation as in Equation 4:

$$F_3(Y) = W_3 * F_2(Y) + B_3 \quad [4]$$

where  $W_3$  with the size of  $n_2 \times f_3 \times f_3$  corresponds to  $c$  filters and  $B_3$ , as  $c$ -dimensional vector.

Then, the image reconstruction output produced better quality images with rich information of high-resolution input for the learning algorithm model.

### Classification of BMT Images

Two datasets were prepared, with one consisting of a control dataset (original images without image reconstruction) and another (reconstructed images by SRCNN). Both datasets contained 600 images, with 200 images for each class split by a ratio of 70% (training): 20% (validation): and 10% (testing) and were fed into the CNN classifier. Cross-validation was applied in parallel with hyperparameter tuning. Subsequently, the average of the test result was taken into consideration. The importance of cross-validation in the model development was to avoid bias in the dataset, whereby the dataset was split randomly and swapped between training, validation, and testing. This strategy allowed the model to learn better of the whole dataset. Consequently, every observation in the dataset appeared in training, thus enabling the model to discover the underlying data distribution. The classifier's output for both datasets was then compared to observe the efficiency of SRCNN.

## RESULTS AND DISCUSSION

### Image Quality Checking

The greyscale images in Figure 6 show the output, which was categorised as 'Blurry', with faded segmentation of blood cells in the bone marrow images. Based on the example shown in the ET class, the output of the Laplacian variance was 28.65. From the greyscale image, the cell separation was seen as unclear. The feature of the megakaryocyte that carried important ET class morphology could not be observed accurately. This low-quality image could disrupt the learning process in developing the classification model as the features could not be differentiated from the background and neighbour cells. Thus, the morphology of the bone marrow that should represent a subtype of MPN could not be identified and may feed inaccurate information to the model. A similar observation was found in the MF class image, where the value of Laplacian variance was 68.32. The fibrosis could be seen roughly, and another detailed feature, such as the presence of megakaryopoiesis for maturation defect in nuclear components, was unclear. Despite being categorised as a blurred image, the value of Laplacian variance was high, approaching 100, which means that more apparent segmentation of the bone marrow image could be observed.

Meanwhile, the PV class has the highest Laplacian variance; more features can be seen in the bone marrow greyscale images. However, the value was still lower than the threshold, and the image was blurry. Details such as erythroid were probably missed, and the dense cellularity can cause the image to be classified as MF class. Therefore, the identified blur images needed to undergo image reconstruction using SRCNN to observe the important morphological features further.

On the other hand, the 'Not Blurry' category is presented in Figure 7, whereby the greyscale image shows clear separability between the cells and their background. The segmentation of the features was identifiable, and the morphology of the MPN subtype

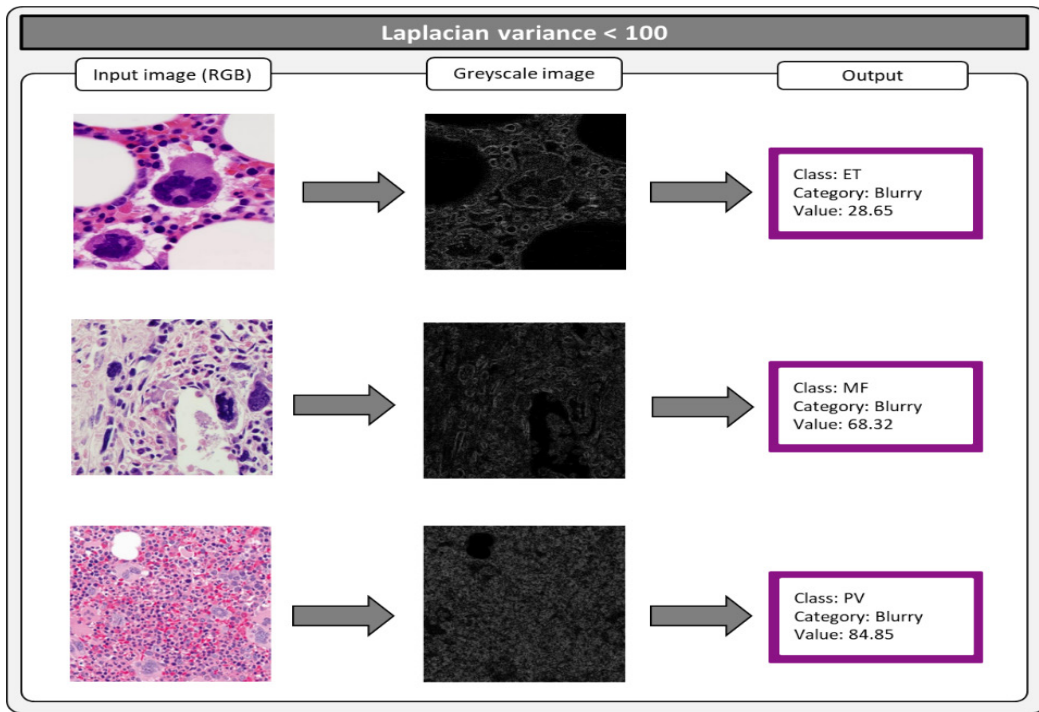


Figure 6. RGB and greyscale image for Laplacian variance <100

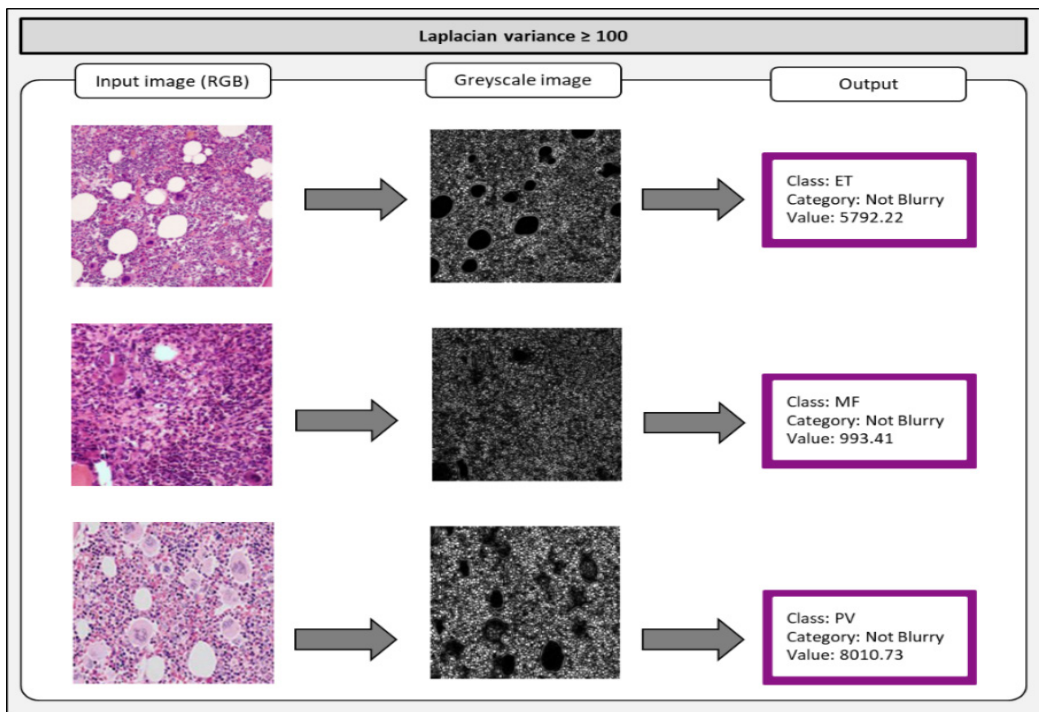


Figure 7. RGB and greyscale images for Laplacian variance  $\geq 100$

in the bone marrow image was well-detected. For example, for the ET class output, the Laplacian variance output was 5,792.22, and the features of the megakaryocytes could be assessed and differentiated from the fat cells in the image effortlessly. More dense cellularity could be seen for both MF and PV classes, with the Laplacian variance output were 993.41 and 8,010.73, respectively. Furthermore, the hyperlobulation nuclear features of the megakaryocytes could be seen clearly, which provided more dominant features of the bone marrow to be identified as PV class. Certainly, good image quality boosts the performance of the classification model in the learning process and produces better results in predicting the output.

### **Application of SRCNN to Blur Images**

An example of bone marrow images for the MF class classified as a blur with a Laplacian variance of less than 100 is shown in Figure 8. For the ET class, the value of the Laplacian variance of 28.65 was recorded before the image reconstruction. After the image reconstruction, the Laplacian variance was increased to 331.65. The segmentation of features or cells in the bone marrow image was hard to be seen as separable in the greyscale image. After the image reconstruction, the segmentation could be observed clearly. Staghorn-like shape to indicate hyperlobulation in nuclear features of megakaryocytes was seen clearer. Another example is that the original Laplacian variance for the MF class was 68.32 and improved to 804.72 after the image reconstruction. Also, the high cellularity of the bone marrow image and a small cluster of megakaryocytes could be observed better after the reconstruction. Similarly, for the image of the PV class, a low value of Laplacian variance (84.85) before the reconstruction increased to 1,010.37 after the reconstruction, which provides a better image in identifying the features of the bone marrow. The hypercellular features, too, could be observed better, and the megakaryocytes that were seen increased in quantity.

Based on the findings, the original low-resolution images with faded and unclear segmentation were transformed into high-resolution images that provided better morphological information to the learning algorithm. The observation from the greyscale images and the output of the Laplacian variance proved the effectiveness of image reconstruction in improving the image quality in the dataset.

### **Classification Performance**

The classification performance was observed using the test dataset and is presented in Table 2. The classification report found that the precision output for the ET class by the control dataset is higher than the SRCNN dataset. A similar result was observed for both SRCNN and control datasets for the MF class, and higher precision output by SRCNN was reported for the PV class. The SRCNN showed better recall or sensitivity for the ET

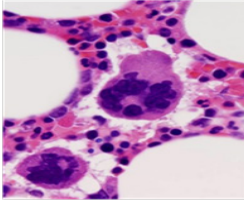
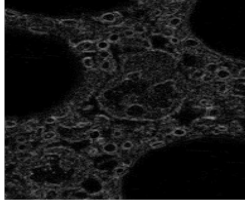
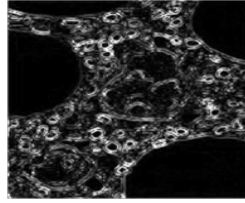
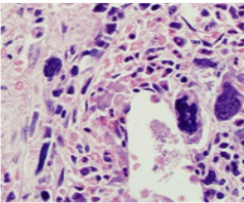
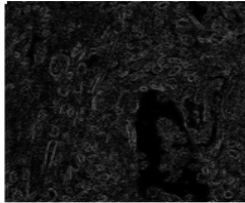
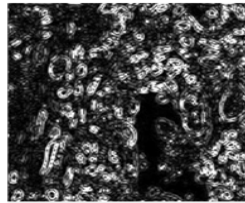
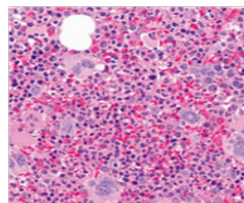
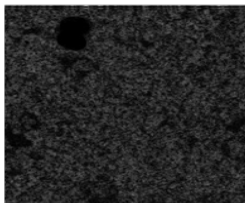
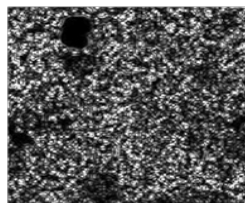
Image Reconstruction		
Class	Before	After
<p>ET</p> 	<p>Value: 28.65</p> 	<p>Value: 331.65</p> 
<p>MF</p> 	<p>Value: 68.32</p> 	<p>Value: 804.72</p> 
<p>PV</p> 	<p>Value: 84.85</p> 	<p>Value: 1010.37</p> 

Figure 8. The output of image reconstruction using SRCNN

Table 2  
Classification report for SRCNN and control dataset

Type of Dataset	Precision			Recall			F1-Score			Accuracy
	ET	MF	PV	ET	MF	PV	ET	MF	PV	
SRCNN	0.89	0.95	0.90	0.85	1.00	0.90	0.87	0.98	0.90	0.92
Control	1.00	0.95	0.77	0.75	0.90	1.00	0.86	0.92	0.87	0.88

and MF classes, but the control dataset provided a better output for the PV class. In the F1-score result, the best outcome was given by the SRCNN dataset for all three classes. Overall, higher accuracy was shown in the SRCNN dataset, with 92% accuracy, compared to the control dataset, with 88% accuracy in classifying the MPN subtypes.

A further observation from the confusion matrix as presented in Figure 9, the SRCNN dataset predicted 17 images of the ET class accurately compared to the control dataset (15 images). The best performance shown by the SRCNN was in the MF class, with all images correctly predicted to true label. Meanwhile, 18 images were classified correctly for the MF

class by the control dataset. However, the control dataset gave the best output to classify 20 images correctly for the PV class, while the SRCNN dataset predicted 18 images correctly. This outcome suggests that the edges of features in the blurry images were softened (Figure 8) before the image reconstruction. It may change the morphology features in the PV class, where the hypercellularity becomes less visible and more generalised. Due to that, the control dataset has a simpler image to classify and produces better output. Overall, the SRCNN dataset shows better output to classify two classes (ET and MF classes) than only one class (PV class) for the control dataset.

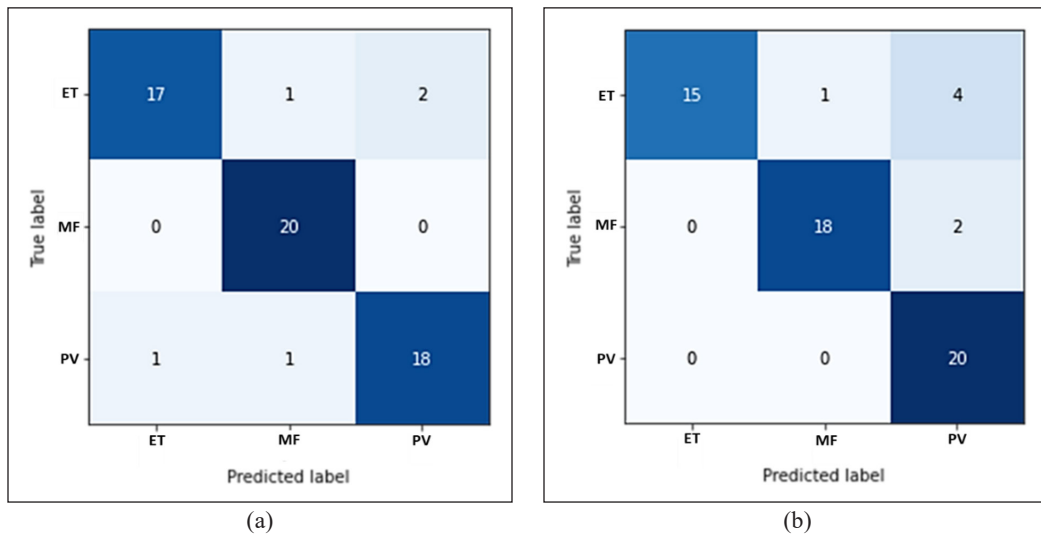


Figure 9. Confusion matrix for: (a) SRCNN; and (b) control

### CONCLUSION

Image quality is a significant practice frequently disregarded in developing a classification model (Dodge & Karam, 2016). Low-quality input images can reduce the ability of the learning algorithm to produce a robust model. Therefore, enhancing blur images from low-quality images is highly significant to be implemented at the early stage of the model development. For instance, a low value of Laplacian variance that indicates blur images can cause difficulties in observing the morphological cells in BMT images that carry major criteria to differentiate MPNs. This situation may reduce information to the learning algorithm in identifying important features from the images. Subsequently, the enhancement of image quality for BMT image from the SRCNN image reconstruction indicated by the improvement of the calculated value of Laplacian variance can produce good quality input data. Hence better accuracy from the output of the prediction model can be observed. Based on the result, the dataset of SRCNN images produced higher results, with an accuracy of 92% compared to the control images (88%). In conclusion, image reconstruction using

SRCNN has proven to effectively improve the quality of BMT images in the pre-processing stage and enhance the performance in the development of the prediction model.

## ACKNOWLEDGEMENT

Umi Kalsom Mohamad Yusof is a PhD student who performed this research. The supervisory committees are Syamsiah Mashohor, Marsyita Hanafi, and Sabariah Md Noor. Nusafina Zainal is a pathologist and prepares clinical data from Hospital Serdang. Clinical data used in this research was approved by the Medical Research and Ethics Committee, Ministry of Health Malaysia (NMRR-18-4023-42507 (IIR)). This research publication is supported by the UPM-Kyutech International Symposium on Applied Engineering and Sciences 2021 (SAES2021) and Universiti Putra Malaysia.

## REFERENCES

- Ali, U., & Mahmood, M. T. (2018). Analysis of blur measure operators for single image blur segmentation. *Applied Sciences*, 8(5), Article 807. <https://doi.org/10.3390/app8050807>
- Alzubaidi, L., Zhang, J., Humaidi, A. J., Al-Dujaili, A., Duan, Y., Al-Shamma, O., Santamaria, J., Fadhel, M. A., Al-Amidie, M., & Farhan, L. (2021). Review of deep learning: concepts, CNN architectures, challenges, applications, future directions. *Journal of Big Data*, 8, Article 53. <https://doi.org/10.1186/s40537-021-00444-8>
- Arber, D. A., Orazi, A., Hasserjian, R., Thiele, J., Borowitz, M. J., Le Beau, M. M., Bloomfield, C. D., Cazzola, M., & Vardiman, J. W. (2016). The 2016 revision to the World Health Organization classification of myeloid neoplasms and acute leukemia. *Blood*, 127(20), 2391-2405. <https://doi.org/10.1182/blood-2016-03-643544>
- Barbui, T., Thiele, J., Gisslinger, H., Kvasnicka, H. M., Vannucchi, A. M., Guglielmelli, P., Orazi, A., & Tefferi, A. (2018). The 2016 WHO classification and diagnostic criteria for myeloproliferative neoplasms: document summary and in-depth discussion. *Blood Cancer Journal*, 8, Article 15. <https://doi.org/10.1038/s41408-018-0054-y>
- Chen, Y., Wang, J., Chen, X., Sangaiah, A. K., Yang, K., & Cao, Z. (2019). Image super-resolution algorithm based on dual-channel convolutional neural networks. *Applied Sciences*, 9(11), Article 2316. <https://doi.org/10.3390/app9112316> (Retraction published 2021, *Applied Sciences*, 11(20), Article 9442)
- Cheng, Z., Sun, H., Takeuchi, M., & Katto, J. (2018). Performance comparison of convolutional autoencoders, generative adversarial networks and super-resolution for image compression. In *Proceedings of the IEEE Conference on Computer Vision and Pattern Recognition Workshops* (pp. 2613-2616). Computer Vision Foundation. <https://doi.org/10.48550/arXiv.1807.00270>
- Dameshek, W. (1951). Some speculations on the myeloproliferative syndromes. *Blood*, 6(4), 372-375. <https://doi.org/10.2307/j.ctvczzbq.35>
- Dodge, S., & Karam, L. (2016). Understanding how image quality affects deep neural networks. In *2016 Eighth International Conference on Quality of Multimedia Experience (QoMEX)* (pp. 1-6). IEEE Publishing. <https://doi.org/10.1109/QoMEX.2016.7498955>

- Hasserjian, R. P. (2018). Changes in the World Health Organization 2016 classification of myeloid neoplasms everyone should know. *Current Opinion in Hematology*, 25(2), 120-128. <https://doi.org/10.1097/MOH.0000000000000404>
- Hayat, K. (2018). Multimedia super-resolution via deep learning: A survey. *Digital Signal Processing*, 81, 198-217. <https://doi.org/10.1016/j.dsp.2018.07.005>
- Hou, J., Si, Y., & Yu, X. (2020). A novel and effective image super-resolution reconstruction technique via fast global and local residual learning model. *Applied Sciences*, 10(5), Article 1856. <https://doi.org/10.3390/app10051856>
- Huang, R., Feng, W., Fan, M., Wan, L., & Sun, J. (2018). Multiscale blur detection by learning discriminative deep features. *Neurocomputing*, 285, 154-166. <https://doi.org/10.1016/j.neucom.2018.01.041>
- Jain, P. A., & Kosamkar, P. K. (2022). Analysis and prediction of COVID-19 with image super-resolution using CNN and SRCNN-Based approach. In T. Senjyu, P. N. Mahalle, T. Perumal & A. Joshi (Eds.), *Smart Innovation, Systems and Technologies: Vol. 248. ICT with Intelligent Applications* (pp. 33-40). Springer. [https://doi.org/10.1007/978-981-16-4177-0\\_5](https://doi.org/10.1007/978-981-16-4177-0_5)
- Leena, M. F., & Sreenath, N. (2019). Pre-processing techniques for detection of blurred images. In N. Chaki, N. Devarakonda, A. Sarkar & N. Debnath (Eds.), *Lecture Notes on Data Engineering and Communications Technologies: Vol. 28. Proceedings of International Conference on Computational Intelligence and Data Engineering* (pp. 59-66). Springer. [https://doi.org/10.1007/978-981-13-6459-4\\_7](https://doi.org/10.1007/978-981-13-6459-4_7)
- Loey, M., Naman, M., & Zayed, H. (2020). Deep transfer learning in diagnosing leukemia in blood cells. *Computers*, 9(2), Article 29. <https://doi.org/10.3390/computers9020029>
- Mariam, K., Afzal, O. M., Hussain, W., Javed, M. U., Kiyani, A., Rajpoot, N., Khurram, S. A., & Khan, H. A. (2022). On smart gaze based annotation of histopathology images for training of deep convolutional neural networks. *IEEE Journal of Biomedical and Health Informatics*, 26(7), 3025-3036. <https://doi.org/10.1109/JBHI.2022.3148944>
- Parsania, P. S., & Virparia, P. V. (2016). A comparative analysis of image interpolation algorithms. *International Journal of Advanced Research in Computer and Communication Engineering*, 5(1), 29-34. <https://doi.org/10.17148/ijarcc.2016.5107>
- Rahaman, M. A., Chen, J., Fu, Z., Lewis, N., Iraj, A., & Calhoun, V. D. (2021). Multi-modal deep learning of functional and structural neuroimaging and genomic data to predict mental illness. In *2021 43<sup>rd</sup> Annual International Conference of the IEEE Engineering in Medicine and Biology Society (EMBC)* (pp. 3267-3272). IEEE Publishing. <https://doi.org/10.1109/EMBC46164.2021.9630693>
- Sirinukunwattana, K., Aberdeen, A., Theissen, H., Sousos, N., Psaila, B., Mead, A. J., Turner, G. D. H., Rees, G., Rittscher, J., & Royston, D. (2019). *Improving the diagnosis and classification of ph-negative myeloproliferative neoplasms through deep phenotyping*. BioRxiv. <https://doi.org/10.1101/762013>
- Talo, M. (2019). Automated classification of histopathology images using transfer learning. *Artificial Intelligence in Medicine*, 101, Article 101743. <https://doi.org/10.1016/j.artmed.2019.101743>
- Taş, M., & Yılmaz, B. (2021). Super resolution convolutional neural network based pre-processing for automatic polyp detection in colonoscopy images. *Computers and Electrical Engineering*, 90, Article 106969. <https://doi.org/10.1016/j.compeleceng.2020.106959>

- Tavares, R. S., Nonino, A., Pagnano, K. B. B., Nascimento, A. C. K. V. d. Conchon, M., Fogliatto, L. M., Funke, V. A. M., Bendit, I., Clementino, N. C. D., Chauffaille, M. d. L. L. F., Bernardo, W. M., & de Souza Santos, F. P. (2019). Guideline on myeloproliferative neoplasms: Associação Brasileira de Hematologia, Hemoterapia e Terapia Celular: Project guidelines: Associação Médica Brasileira - 2019. *Hematology, Transfusion and Cell Therapy*, 41(Supplement 1), 1-73. <https://doi.org/10.1016/j.htct.2019.03.001>
- Umehara, K., Ota, J., & Ishida, T. (2018). Application of super-resolution convolutional neural network for enhancing image resolution in chest CT. *Journal of Digital Imaging*, 31, 441-450. <https://doi.org/10.1007/s10278-017-0033-z>
- Vannucchi, A. M., & Harrison, C. N. (2017). Emerging treatments for classical myeloproliferative neoplasms. *Blood*, 129(6), 693-703. <https://doi.org/10.1182/blood-2016-10-695965>
- Vasudevan, S., Saha, A., Tarver, M. E., & Patel, B. (2022). Digital biomarkers: Convergence of digital health technologies and biomarkers. *Npj Digital Medicine*, 5, Article 36. <https://doi.org/10.1038/s41746-022-00583-z>
- Zhang, H. M., & Dong, B. (2020). A review on deep learning in medical image reconstruction. *Journal of the Operations Research Society of China*, 8, 311-340. <https://doi.org/10.1007/s40305-019-00287-4>
- Zhang, J., Shao, M., Yu, L., & Li, Y. (2020). Image super-resolution reconstruction based on sparse representation and deep learning. *Signal Processing: Image Communication*, 87, Article 115925. <https://doi.org/10.1016/j.image.2020.115925>